

The following resources related to this article are available online at www.sciencemag.org (this information is current as of October 8, 2009):

Updated information and services, including high-resolution figures, can be found in the online version of this article at:

<http://www.sciencemag.org/cgi/content/full/326/5950/272>

Supporting Online Material can be found at:

<http://www.sciencemag.org/cgi/content/full/326/5950/272/DC1>

This article has been **cited by** 1 articles hosted by HighWire Press; see:

<http://www.sciencemag.org/cgi/content/full/326/5950/272#otherarticles>

This article appears in the following **subject collections**:

Physics

<http://www.sciencemag.org/cgi/collection/physics>

Information about obtaining **reprints** of this article or about obtaining **permission to reproduce this article** in whole or in part can be found at:

<http://www.sciencemag.org/about/permissions.dtl>

26. J. R. Maze *et al.*, *Nature* **455**, 644 (2008).
 27. G. Balasubramanian *et al.*, *Nature* **455**, 648 (2008).
 28. J. M. Taylor *et al.*, *Nat. Phys.* **4**, 810 (2008).
 29. N. Khaneja, T. Reiss, C. Kehlet, T. Schulte-Herbruggen, S. J. Glaser, *J. Magn. Reson.* **172**, 296 (2005).
 30. P. Cappellaro, L. Jiang, J. S. Hodges, M. D. Lukin, *Phys. Rev. Lett.* **102**, 210502 (2009).
 31. N. B. Manson, J. P. Harrison, M. J. Sellars, *Phys. Rev. B* **74**, 104303 (2006).
 32. A. Batalov *et al.*, *Phys. Rev. Lett.* **102**, 195506 (2009).
 33. We thank P. Cappellaro, L. Childress, J. Doyle, M. V. G. Dutt, J. MacArthur, A. Sorenson, P. Stanwix, E. Togan, and A. Trifonov for many stimulating discussions and experimental help. This work was supported by the Defense Advanced Research Projects Agency, NSF, the Packard Foundation, and the Pappalardo Fellowship. The content of the information does not necessarily reflect the position or the policy of the U.S. Government, and no official endorsement should be inferred.

Supporting Online Material

www.sciencemag.org/cgi/content/full/1176496/DC1
 Materials and Methods
 Figs. S1 to S4
 References

19 May 2009; accepted 29 July 2009
 Published online 10 September 2009;
 10.1126/science.1176496
 Include this information when citing this paper.

Persistent Currents in Normal Metal Rings

A. C. Bleszynski-Jayich,¹ W. E. Shanks,¹ B. Peaudecerf,¹ E. Ginossar,¹ F. von Oppen,² L. Glazman,^{1,3} J. G. E. Harris^{1,3}

Quantum mechanics predicts that the equilibrium state of a resistive metal ring will contain a dissipationless current. This persistent current has been the focus of considerable theoretical and experimental work, but its basic properties remain a topic of controversy. The main experimental challenges in studying persistent currents have been the small signals they produce and their exceptional sensitivity to their environment. We have developed a technique for detecting persistent currents that allows us to measure the persistent current in metal rings over a wide range of temperatures, ring sizes, and magnetic fields. Measurements of both a single ring and arrays of rings agree well with calculations based on a model of non-interacting electrons.

An electrical current induced in a resistive circuit will rapidly decay in the absence of an applied voltage. This decay reflects the tendency of the circuit's electrons to dissipate energy and relax to their ground state. However, quantum mechanics predicts that the electrons' many-body ground state (and, at finite temperature, their thermal equilibrium state) may contain a persistent current (PC), which flows through the resistive circuit without dissipating energy or decaying. A dissipationless equilibrium current flowing through a resistive circuit is counterintuitive, but it has a familiar analog in atomic physics: Some atomic species' electronic ground states possess nonzero orbital angular momentum, which is equivalent to a current circulating around the atom.

One of the major insights of mesoscopic condensed-matter physics is that this analogy remains valid even when the electrons experience a static disorder potential, as in a resistive metal (*I*). Theoretical treatments of PCs in resistive metal rings have been developed over a number of decades [see (1, 2) and references therein]. Calculations that take into account the electrons' inevitable coupling to the static disorder potential and a fluctuating thermal bath predict several general features. A micrometer-diameter ring will support a PC of $I \sim 1$ nA at temperatures $T \lesssim 1$ K. A magnetic flux Φ threading the ring will break time-reversal symmetry, allowing the PC to flow in a particular direction around the ring. Furthermore, the Aharonov-Bohm effect will require I to be pe-

riodic in Φ with period $\Phi_0 = h/e$, thereby providing a clear-cut experimental signature of the PC.

These predictions have attracted considerable interest, but measuring the PC is challenging for a number of reasons. For example, the PC flows only within the ring and so cannot be measured with a conventional ammeter. Experiments to date (2, 3) have mostly used superconducting quantum interference devices (SQUIDs) to infer the PC from the magnetic field it produces. Interpretation of these measurements has been complicated by the SQUID's low signal-to-noise ratio (SNR) and the uncontrolled back action of the SQUID's ac Josephson oscillations, which may drive nonequilibrium currents in the rings. In addition, SQUIDs perform optimally in low magnetic fields; this limits the maximum Φ that can be applied to the rings, allowing observation of only a few oscillations of $I(\Phi)$ and complicating the subtraction of background signals unrelated to the PC.

Experiments to date have produced a number of confusing results in apparent contradiction with theory and even among the experiments themselves (2, 3). These conflicts have remained without a clear resolution for nearly 20 years, suggesting that our understanding of how to measure and/or calculate the ground-state properties of as simple a system as an isolated metal ring may be incomplete.

More recent theoretical work has predicted that the PC is highly sensitive to a variety of subtle effects, including electron-electron interactions (4–7), the ring's coupling to its electromagnetic environment (8), and trace magnetic impurities within the ring (9). These theories have not explained all of the experimental results to date, but they do indicate that accurate measurements of the PC would be able to address a number of interesting questions in many-body

condensed-matter physics (in addition to resolving the long-standing controversy described above).

We measured the PC in resistive metal rings using a micromechanical detector with orders of magnitude greater sensitivity and lower back-action than SQUID-based detectors. Our approach allows us to measure the PC in a single ring and arrays of rings as a function of ring size, temperature, and the magnitude and orientation of the magnetic field over a much broader range than has been possible previously. Quantitative agreement is found between these measurements and calculations based on a model of diffusive, non-interacting electrons. This agreement is supported by independent measurements of the rings' electrical properties.

Figure 1, A to C, shows single-crystal Si cantilevers with integrated Al rings [their fabrication is described elsewhere (10)]. All the PC measurements were made in magnetic fields well above the critical field of Al, ensuring that the rings were in their normal (rather than superconducting) state. The parameters of the four ring samples measured are given in Table 1.

In the presence of a magnetic field \vec{B} , each ring's current I produces a torque on the cantilever $\vec{\tau} = \vec{\mu} \times \vec{B}$ as well as a shift δv in the cantilever's resonant frequency v . Here $\vec{\mu} = \pi r^2 I \hat{n}$ is the magnetic moment of the PC, r is the ring radius, and \hat{n} is the unit vector normal to the ring. We infer $I(B)$ from measurements of $\delta v(B)$; the conversion between $\delta v(B)$ and $I(B)$ is described in the supporting online material (SOM) text.

To monitor v , we drive the cantilever in a phase-locked loop. The cantilever is driven via a piezoelectric element, and the cantilever's displacement is monitored by a fiber-optic interferometer (11). The cantilever's thermally limited force sensitivity is ~ 2.9 aN/Hz^{1/2} at $T = 300$ mK, corresponding to a magnetic moment sensitivity of ~ 11 μ_B /Hz^{1/2} and a current sensitivity of ~ 20 pA/Hz^{1/2} for a ring with $r = 400$ nm at $B = 8$ T. By comparison, SQUID magnetometers achieve a current sensitivity $\gtrsim 5$ nA/Hz^{1/2} for a similar ring (12–14). The noise temperature of the cantilever and the electron temperature of a metal sample at the end of a cantilever both equilibrate with the fridge temperature for the conditions we used (11).

The frequency shift of a cantilever containing an array of $N = 1680$ lithographically identical rings with $r = 308$ nm at $T = 323$ mK is shown (Fig. 1D) as a function of B . Oscillations with a period ~ 20 mT, corresponding to a flux h/e through each ring, are visible in the raw data. Depending on r and θ (the angle between \vec{B} and the plane of

¹Department of Physics, Yale University, New Haven, CT 06520, USA. ²Institut für Theoretische Physik, Freie Universität Berlin, Fachbereich Physik, 14195 Berlin, Germany. ³Department of Applied Physics, Yale University, New Haven, CT 06520, USA.

the ring), we observe as many as 450 oscillations over a 5.5-T range of B (figs. S12 to S17).

Figure 1E shows the data from Fig. 1D after subtracting the smooth background and converting the data from $\delta\nu(B)$ to $I(B)$ using the expressions in the SOM text. The lefthand axis in Fig. 1E shows the total PC inferred from the measurement, which is the sum of the PC from each ring in the array. The righthand axis shows the estimated typical single-ring PC: $I_{\text{typ}} = I_{\Sigma}/\sqrt{N}$. This relationship between I_{typ} and I_{Σ} arises because the PC in each ring is predicted to oscillate as a function of B with a phase that depends on the ring's microscopic disorder, and thus is assumed to be random from ring to ring. This assumption is verified below.

To establish that $\delta\nu$ provides a reliable measure of the PC, $I_{\text{typ}}(B)$ was measured as a function of several experimental conditions: the laser power incident on the cantilever, the amplitude and frequency of the cantilever's motion, the polarity and orientation of the magnetic field, and the presence or absence of room-temperature electronics connected to the cryostat. These data are shown in the SOM text and indicate that the measurements of $I_{\text{typ}}(B)$ are independent of these parameters (for the conditions of our experiment) and reflect the equilibrium PC in the rings.

Figure 2, A to C, shows $I_{\text{typ}}(B)$ for arrays of rings with three different radii: $r = 308, 418,$ and 793 nm. We have also measured a single ring with $r = 418$ nm (Fig. 2D). Figure 2, E to H, shows $|\tilde{I}_{\text{typ}}(f_{\Phi})|$, the absolute value of the Fourier transform of the data in Fig. 2, A to D [f_{Φ} is the flux frequency in units of $(h/e)^{-1}$]. Figure 2, I to L, shows $G_{\text{typ}}(\delta B)$, the autocorrelation of $I_{\text{typ}}(B)$ for each of these samples. $G_{\text{typ}}(\delta B)$ is calculated from measurements of $I_{\text{typ}}(B)$ taken over a much broader range of B than is shown in Fig. 2, A to D; the complete data are shown in the SOM text.

A number of conclusions can be drawn from a qualitative examination of these data. First, $I_{\text{typ}}(B)$ oscillates with a period $\approx h/e$ but also contains an aperiodic modulation that broadens the peaks in $\tilde{I}_{\text{typ}}(f_{\Phi})$ and causes $G_{\text{typ}}(\delta B)$ to decay at large δB . This modulation is due to the fact that we apply a uniform B to the sample, leading to magnetic flux inside the metal of each ring given by $\Phi_M = BA_M$ where A_M is the area of the metal projected along \vec{B} . This leads to a new effective disorder potential [and hence a randomization of the phase of the $I(B)$ oscillations] each time Φ_M changes by $\sim\Phi_0$ (15). As a result, the peaks in $\tilde{I}_{\text{typ}}(f_{\Phi})$ span a band of f_{Φ} roughly bounded by the rings' inner and outer radii (the blue bars in Fig. 2, E to H), and the decay of $G_{\text{typ}}(\delta B)$ is found to occur on a field scale [defined as the half width at half maximum of $G_{\text{typ}}(\delta B)$] $B_c = \kappa\Phi_0/A_M$. Here κ is a constant that is predicted (16) to be ≈ 1 ; we find $1 < \kappa < 3$ in these samples. For the array samples, ring-to-ring variations in r (estimated to be $\sim 1\%$) should contribute negligibly to B_c and the peak widths in $\tilde{I}_{\text{typ}}(f_{\Phi})$. The fact that the $r = 418$ nm array and the $r = 418$ nm single ring show similar peak

width and B_c indicates that ring-to-ring variations in r do not affect the signal appreciably.

It is clear from Fig. 2 that the PC is smaller in larger rings. This is consistent with the prediction (17) that the typical amplitude $I_{h/e}(T=0)$ of the h/e -periodic Fourier component of $I(\Phi)$ at $T=0$ corresponds roughly to the current produced by a single electron diffusing around the ring at the Fermi energy, and hence should scale as $1/r^2$. In addition, $I_{h/e}(T)$ is predicted (17) to decrease on a temperature scale (known as the Thouless temperature) $T_T \propto 1/r^2$, corresponding to the scale of disorder-induced correlations in the ring's spectrum of single-electron states.

Fig. 1. (A) Cantilever torque magnetometry schematic. An array of metal rings is integrated onto the end of a cantilever. The cantilever is mounted in a ^3He refrigerator. A magnetic field B is applied at an angle θ from the plane of the rings. The out-of-plane component of B provides magnetic flux Φ through the ring. The in-plane component of B exerts a torque on the rings' magnetic moment and causes a shift in the cantilever's resonant frequency $\delta\nu$. Laser interferometry is used to monitor the cantilever's motion and to determine $\delta\nu$. (B) A scanning electron micrograph of several Si cantilevers similar to those used in the experiment. The light regions at the end of some of the cantilevers are arrays of Al rings. The individual rings are visible in (C), which shows a magnified view of the region in (B) outlined in red. (D) Raw data showing $\delta\nu$ as a function of B for an array of $N = 1680$ rings with $r = 308$ nm at $T = 365$ mK and $\theta = 45^\circ$. (E) PC inferred from the frequency shift data in (D) after subtracting a smooth background from the raw data. The lefthand axis shows the total current I_{Σ} in the array, and the righthand axis shows the estimated typical per-ring current $I_{\text{typ}} = I_{\Sigma}/\sqrt{N}$. Oscillations with a characteristic period of ~ 20 mT (corresponding to $\Phi = h/e$) are visible in (D) and (E).

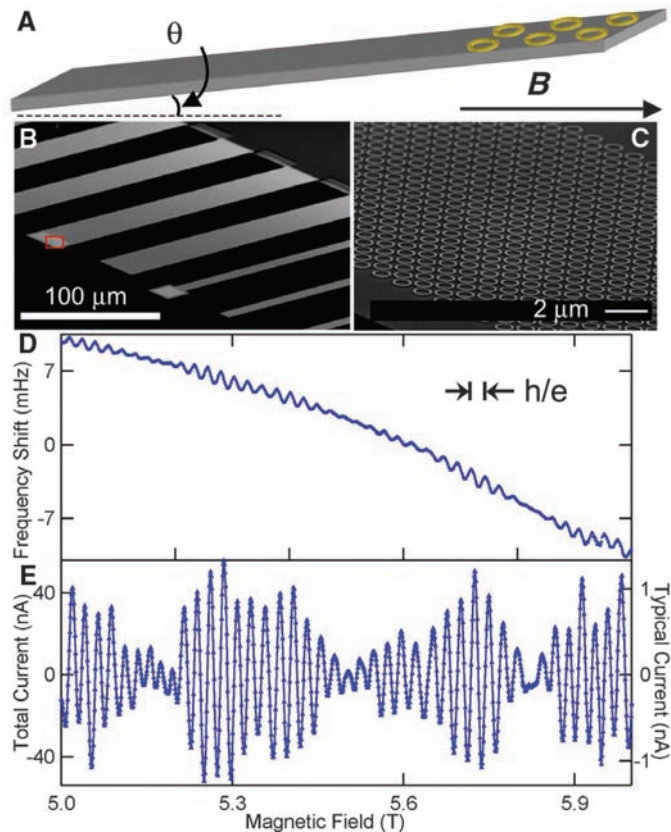
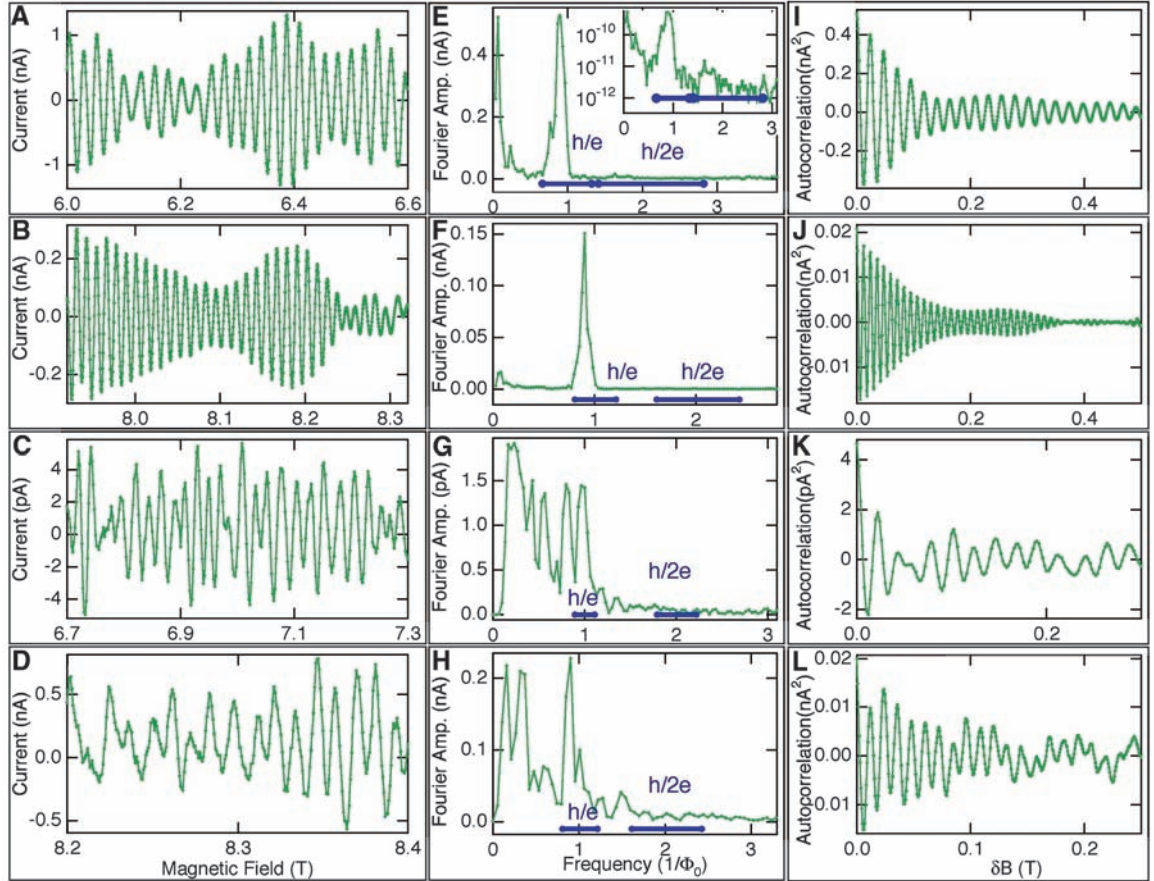


Table 1. Sample parameters. For each of the four ring samples, the rings' mean radius r , linewidth w , and thickness d are listed, along with the number N of rings in the sample. The electrons' diffusion constant D , extracted from the fits in Fig. 3, is given. The stated errors are statistical errors in the fits. An additional 6% error in D is estimated for uncertainties in the overall calibration, as discussed in the SOM text. The fifth sample is the codeposited wire used in the transport measurements described in the SOM text. For this sample, D was determined from the wire's resistivity.

Sample	r (nm)	w (nm)	d (nm)	N	D (cm^2/s)
308-nm array	308	115	90	1680	271 ± 2.6
418-nm array	418	85	90	990	214 ± 3.3
793-nm array	793	85	90	242	205 ± 6.5
418-nm ring	418	85	90	1	215 ± 4.6
Wire (see SOM text)	289,000 (length)	115	90	1	260 ± 12

Fig. 2. PC versus magnetic field in (A) the 308-nm array for $T = 365$ mK, $\theta = 45^\circ$; (B) the 418-nm array for $T = 365$ mK, $\theta = 45^\circ$; (C) the 793-nm array for $T = 323$ mK, $\theta = 6^\circ$; and (D) the 418-nm ring for 365 mK, $\theta = 45^\circ$. In each case, a smooth background has been removed. (E to H) Fourier transforms of the data in (A) to (D). The expected h/e and $h/2e$ periodicities are indicated by the horizontal blue bars. The bars' widths reflect the rings' linewidth w . A small $h/2e$ peak is present in (E) (visible in the log-scale graph, inset). (I to L) The autocorrelation functions of the data shown in (A) to (D), but computed over a field range ΔB larger than shown in (A) to (D): $\Delta B =$ (I) 5.4 T, (J) 5.3 T, (K) 0.6 T, and (L) 1.1 T (full data are shown in the SOM text).



length $\ell_B = \sqrt{\hbar/eB}$, which for this experiment should render $I_{\Sigma}^{\text{(avg)}}$ unobservably small. As a result, the peak in Fig. 2E at $f_{\Phi} = 2$ presumably reflects the random component of the second harmonic of $I(\Phi)$, which is predicted (17) to have a zero-temperature amplitude $I_{h/2e}(0) = I_{h/e}(0)/2^{3/2}$, to be suppressed on a temperature scale $= T_T/4$, and to produce a signal with the same \sqrt{N} scaling as $I_{h/e}$.

We now turn to a more quantitative analysis of the data. Theory predicts (17) that, for each independent realization of the disorder potential, $I_{h/pe}$ [the p^{th} harmonic of $I(\Phi)$] is drawn randomly from a distribution with a mean $\langle I_{h/pe} \rangle = 0$ and a root mean square (rms) value $\langle I_{h/pe}^2 \rangle^{1/2}$, which in general is nonzero. Here $\langle \dots \rangle$ represents an average over disorder potentials. The quantity $\langle I_{h/pe}^2 \rangle^{1/2}$ can be calculated explicitly as a function of r , T , p , and the electrons' diffusion constant D for a variety of models.

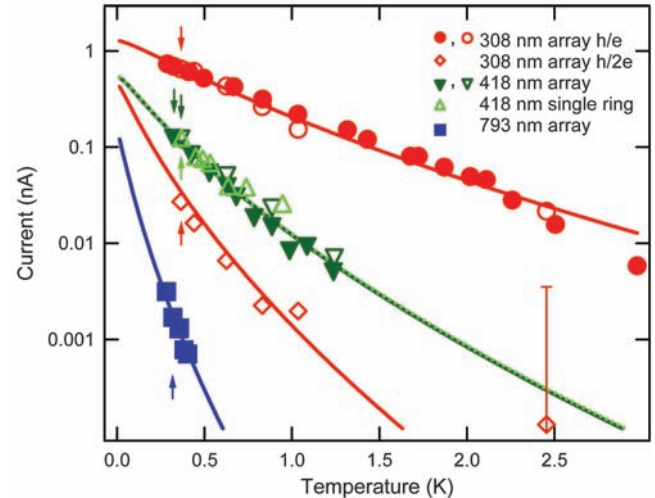
To compare our data against these calculations, we make use of the fact that $\langle I_{h/pe}^2 \rangle^{1/2}$ can be extracted from a measurement of $I_{\Sigma}(B)$ when the measurement record spans many B_c . When this condition is satisfied, averages performed with respect to B are equivalent to averages performed with respect to disorder realizations, and it is straightforward to show that the area under a peak in $|\tilde{I}_{\text{typ}}(f_{\Phi})|^2$ (Fig. 2, E to H) at $f_{\Phi} = p$ is simply related to $\langle I_{h/pe}^2 \rangle^{1/2}$

Fig. 3. Temperature dependence of the h/e and $h/2e$ Fourier components of the current per ring. The vertical axis indicates $\langle I_{h/e}^2 \rangle^{1/2}$ and $\langle I_{h/2e}^2 \rangle^{1/2}$, the rms values of the Fourier amplitudes of the persistent current. In each data set, the open points were taken with $\theta = 45^\circ$, whereas for the solid points, $\theta = 6^\circ$. The arrows indicate the data points derived from $I(B)$ measurements taken over a magnetic field range much greater than B_c ; other data points are derived from the scaling of $I(B)$ measured over a smaller range of B , as described in the SOM text.

The lines (solid for array samples, dotted for the single ring) are fits to the prediction for non-interacting diffusive electrons. The electron diffusion constant D is the only fitting parameter and is listed in Table 1.

$$\left[(f_{\Phi}^+ - f_{\Phi}^-)^{-1} \int_{f_{\Phi}^-}^{f_{\Phi}^+} (|\tilde{I}_{\text{typ}}(f_{\Phi})|^2 - b(f_{\Phi})) df_{\Phi} \right]^{1/2} = \langle I_{h/pe}^2 \rangle^{1/2} \quad (1)$$

Here b is the noise floor in $|\tilde{I}_{\text{typ}}(f_{\Phi})|^2$ and is estimated from the portions of the data away from the peaks. We take the limits of integration



f_{Φ}^+ and f_{Φ}^- to be roughly the values of f_{Φ} corresponding to h/pe flux periodicity through the outer and inner radii of the ring, respectively. In previous experiments, $\langle I_{h/pe}^2 \rangle$ could only be determined by measuring several rings, one ring at a time (3, 20). This approach was limited by the low SNR achieved in single-ring measurements and practical limits on the number of nominally identical rings (≈ 15) that could be measured.

Measurements of $\langle I_{h/e}^2 \rangle^{1/2}$ for each sample and $\langle I_{h/2e}^2 \rangle^{1/2}$ for the smallest rings are shown as a function of T for $\theta = 45^\circ$ (open symbols) and $\theta = 6^\circ$ (solid symbols) (Fig. 3). It can be seen that the PC in larger rings decays more quickly with T than in smaller rings, and that $\langle I_{h/2e}^2 \rangle^{1/2}$ decays more quickly than $\langle I_{h/e}^2 \rangle^{1/2}$, which is consistent with the discussion above. In addition, the agreement between the data for the $r = 418$ nm array and the $r = 418$ nm single ring indicates that the PC signal scales as \sqrt{N} and hence that the PC is random from ring to ring.

The solid lines are fits to theoretical predictions in which $\langle I_{h/pe}^2 \rangle^{1/2}$ is calculated for diffusive non-interacting electrons. This calculation closely follows that of (17) but takes into account the presence of the large magnetic field B inside the metal (which lifts the spin degeneracy and breaks time-reversal symmetry) as well as spin-orbit scattering (the rings' circumference exceeds the spin-orbit scattering length, as discussed in the SOM text). We find

$$\langle I_{h/pe}^2(T) \rangle = g \left(p^2 \frac{T}{T_T} \right) \langle I_{h/pe}^2(0) \rangle \quad (2)$$

$$\text{where } g(x) = \frac{\pi^6}{3} x^2 \sum_{n=1}^{\infty} n \exp[-(2\pi^3 nx)^{1/2}],$$

$$\langle I_{h/pe}^2(0) \rangle^{1/2} = 0.37 p^{-3/2} \frac{3eD}{(2\pi r)^2}, \text{ and } T_T = \frac{\hbar^2 D}{k_B (2\pi r)^2}.$$

The data from each sample were fit separately, in each case using D as the only fitting parameter. The best-fit values of D are listed in Table 1. These values are typical for high-purity evaporated Al wires of the dimensions used here (21, 22); however, to further constrain the comparison between our data and theory, we also independently determined D from the resistivity of a co-deposited wire (the wire's properties are listed in Table 1). This measurement is described in detail in the SOM text and provides a value of D in good agreement with the values extracted from the PC measurements. The values of D in Table 1 show a correlation with the samples' linewidths, which may reflect the increased contribution of surface scattering in the narrower samples.

The calculation leading to Eq. 2 assumes the phase-coherent motion of free electrons around the ring. Measurements of the phase coherence length $L_\phi(T)$ in the co-deposited wire are described in the SOM text and show that $L_\phi \gg 2\pi r$ for nearly all the temperatures at which the PC is observable. The closest approach between L_ϕ and $2\pi r$ at a temperature where the PC can still be observed occurs in the 308-nm array at $T = 3$ K, where we find $L_\phi(3 \text{ K}) = 1.86 \times (2\pi r)$. It is conceivable that the more rapid decrease in $\langle I_{h/e}^2 \rangle^{1/2}$ observed in this sample above $T = 2$ K (Fig. 3) is due to dephasing; however, it is not possible to test this hypothesis in the other samples, because the larger rings' PC is well below the noise floor when $L_\phi(T) = 1.86 \times (2\pi r)$. To the best of our knowledge the effect of dephasing on the PC has not been calculated.

Our measurement of the PC in normal metal rings over a wide range of temperatures, ring sizes, array sizes, magnetic field magnitudes, and magnetic field orientations with high SNR, excellent background rejection, and low measurement back-action indicates that the rings' equilibrium state is well described by the diffusive non-interacting electron model. In addition to providing a clear experimental picture of PCs in simple metallic rings, these results open the possibility of using measurements of the PC to search for ultra-low temperature phase transitions (6) or to study a variety of many-body and environmental effects relevant to quantum phase transitions and quantum coherence in solid-state qubits (23, 24). Furthermore, the micro-mechanical detectors used here are well suited to studying the PC in circuits driven out of equilibrium (for example, by the controlled introduction of microwave radiation) (8). The properties of PCs in these regimes have received relatively little attention to date but could offer new insights into the behavior of isolated nanoelectronic systems.

References and Notes

1. M. Buttiker, I. Imry, R. Landauer, *Phys. Lett.* **96A**, 365 (1983).
2. L. Saminadayar, C. Bäuerle, D. Mailly, *Encycl. Nanosci. Nanotech* **3**, 267 (2004).
3. H. Bluhm, N. C. Koschnick, J. A. Bert, M. E. Huber, K. A. Moler, *Phys. Rev. Lett.* **102**, 136802 (2009).
4. V. Ambegaokar, U. Eckern, *Phys. Rev. Lett.* **65**, 381 (1990).
5. V. Ambegaokar, U. Eckern, *Europhys. Lett.* **13**, 733 (1990).
6. H. Bary-Soroker, O. Entin-Wohlman, Y. Imry, *Phys. Rev. Lett.* **101**, 057001 (2008).
7. U. Eckern, P. Schwab, *Adv. Phys.* **44**, 387 (1995).
8. V. E. Kravtsov, V. I. Yudson, *Phys. Rev. Lett.* **70**, 210 (1993).
9. P. Schwab, U. Eckern, *Z. Phys. B* **103**, 97 (1997).

10. A. C. Bleszynski-Jayich, W. E. Shanks, R. Ilic, J. G. E. Harris, *J. Vac. Sci. Technol. B* **26**, 1412 (2008).
11. A. C. Bleszynski-Jayich, W. E. Shanks, J. G. E. Harris, *Appl. Phys. Lett.* **92**, 013123 (2008).
12. E. M. Q. Jariwala, P. Mohanty, M. B. Ketchen, R. A. Webb, *Phys. Rev. Lett.* **86**, 1594 (2001).
13. M. E. Huber *et al.*, *Rev. Sci. Instrum.* **79**, 053704 (2008).
14. D. Mailly, C. Chapelier, A. Benoit, *Phys. Rev. Lett.* **70**, 2020 (1993).
15. W. J. Skocpol *et al.*, *Phys. Rev. Lett.* **56**, 2865 (1986).
16. P. A. Lee, A. D. Stone, H. Fukuyama, *Phys. Rev. B* **35**, 1039 (1987).
17. E. K. Riedel, F. von Oppen, *Phys. Rev. B* **47**, 15449 (1993).
18. L. P. Levy, G. Dolan, J. Dunsmuir, H. Bouchiat, *Phys. Rev. Lett.* **64**, 2074 (1990).
19. B. L. Altshuler, Y. Gefen, Y. Imry, *Phys. Rev. Lett.* **66**, 88 (1991).
20. V. Chandrasekhar *et al.*, *Phys. Rev. Lett.* **67**, 3578 (1991).
21. P. LaFarge, P. Joyez, D. Esteve, C. Urbina, M. H. Devoret, *Nature* **365**, 422 (1993).
22. C. Song *et al.*, *Phys. Rev. B* **79**, 174512 (2009).
23. P. Cedraschi, V. V. Ponomarenko, M. Büttiker, *Phys. Rev. Lett.* **84**, 346 (2000).
24. A. Kopp, K. Le Hur, *Phys. Rev. Lett.* **98**, 220401 (2007).
25. We thank M. Devoret, R. Ilic, T. Ojanen, and J. C. Sankey for their assistance. A.C.B.-J., W.E.S., and J.G.E.H. are supported by NSF grants 0706380 and 0653377. F.v.O. is supported in part by the Deutsche-Israelische Projektkooperation. J.G.E.H. acknowledges support from the Sloan Foundation. A.C.B.-J. acknowledges support from UNESCO-L'Oreal. L.G. is supported in part by U. S. Department of Energy grant DE-FG02-08ER46482. F.v.O. and L.G. acknowledge the hospitality of the Kavli Institute for Theoretical Physics in the final stages of this work.

Supporting Online Material

www.sciencemag.org/cgi/content/full/326/5950/272/DC1
SOM Text

Figs. S1 to S18

References and Notes

23 June 2009; accepted 8 September 2009

10.1126/science.1178139

The Shape and Surface Variation of 2 Pallas from the Hubble Space Telescope

B. E. Schmidt,^{1*} P. C. Thomas,² J. M. Bauer,³ J.-Y. Li,⁴ L. A. McFadden,⁴ M. J. Mutchler,⁵ S. C. Radcliffe,⁶ A. S. Rivkin,⁷ C. T. Russell,¹ J. Wm. Parker,⁸ S. A. Stern⁸

We obtained Hubble Space Telescope images of 2 Pallas in September 2007 that reveal distinct color and albedo variations across the surface of this large asteroid. Pallas's shape is an ellipsoid with radii of 291 (± 9), 278 (± 9), and 250 (± 9) kilometers, implying a density of 2400 (± 250) kilograms per cubic meter—a value consistent with a body that formed from water-rich material. Our observations are consistent with the presence of an impact feature, 240 (± 25) kilometers in diameter, within Pallas's ultraviolet-dark terrain. Our observations imply that Pallas is an intact protoplanet that has undergone impact excavation and probable internal alteration.

In the current paradigm, the largest asteroids were among the first solar system bodies to form and were the building blocks of planets [e.g., (1) and references therein]. Pallas is the second largest and third most massive asteroid, with a mean radius of 272 km; 1 Ceres is 475 km (2) and 4 Vesta is 265 km (3). These three bodies are the archetypes of their spectral classes: Ceres is the largest of the rare G-types, Vesta is the likely parent body of the Vestoid V-type asteroids and the associated howardite, eucrite, and diogenite (HED) meteorites [e.g., (1)], and Pallas is the largest of the B-types. Like Vesta, Pallas is linked

to an orbital family sharing its orbital and spectral parameters. The largest of these is 5222 Ioffe, with a diameter of 22 km (4). It is assumed that

¹Institute of Geophysics and Planetary Physics, University of California, Los Angeles, CA 90095, USA. ²Department of Astronomy, Cornell University, Ithaca, NY 14853, USA. ³Jet Propulsion Laboratory, Pasadena, CA 91109, USA. ⁴Department of Astronomy, University of Maryland, College Park, MD 20742, USA. ⁵Space Telescope Science Institute (STScI), Baltimore, MD 80302, USA. ⁶Hydralux, Santa Monica, CA 90401, USA. ⁷Applied Physics Laboratory, Laurel, MD 20723, USA. ⁸Southwest Research Institute, Boulder, CO 80302, USA.

*To whom correspondence should be addressed. E-mail: britneys@ucla.edu